

RESEARCH

Open Access



Cross-talk between cuproptosis and ferroptosis to identify immune landscape in cervical cancer for mRNA vaccines development

Xuchao Zhang^{1,2†}, Wenwen Xu^{1,2†}, Zi Wang², Jing Liu², Han Gong^{1,2*} and Wen Zou^{1*}

Abstract

Messenger RNA (mRNA)-based vaccines present a promising avenue for cancer immunotherapy; however, their application in cervical cancer remains unexplored. This study investigated the interplay between the regulated cell death pathways of cuproptosis and ferroptosis to advance the development of mRNA vaccines for cervical cancer. We identified key cuproptosis-related and ferroptosis-related genes (CFRGs) from public mRNA profiles and determined their prognostic significance, mutation frequencies, and effect on the immune landscape. Our analysis revealed two distinct subtypes of cervical cancer associated with CFRGs, with differences in prognosis and immune characteristics. Using LASSO, XGBoost, and SVM-RFE methods, we established a 4-gene prognostic signature (TSC22D3, SQLE, ZNF419, and TFRC) to stratify patients based on their risk and determine its correlation with immune microenvironment, mutation profiles, and treatment responses. RT-qPCR validation confirmed the differential expression of these genes in clinical samples. Our findings identify TSC22D3, SQLE, ZNF419, and TFRC as candidate targets for mRNA vaccine development and offer a potential prognostic tool for personalized cervical cancer treatment.

Keywords mRNA vaccines, Cuproptosis, Ferroptosis, Immunotherapy, Prognosis, Cervical cancer

Introduction

Cervical cancer remains a significant global health

challenge, ranking as the fourth most common cancer among women worldwide [1]. Despite advances in therapeutic strategies, the complex nature of cervical cancer necessitates a deeper insight to improve prognostic assessment and achieve tailored therapeutic interventions [2]. Prognostic biomarkers, particularly those exploring the molecular complexity of cell death pathways, have shown promise in refining risk stratification and guiding personalized treatment strategies [3–5].

Cancer vaccines reactivate the immune system against tumor cells with low toxicity and durable efficacy, making them promising for widespread clinical application [6, 7]. mRNA vaccines have gained much attention due

[†]Xuchao Zhang and Wenwen Xu have contributed equally to this work.

*Correspondence:

Han Gong

hangong@csu.edu.cn

Wen Zou

zouwen29w@csu.edu.cn

¹ Department of Oncology, The Second Xiangya Hospital, Central South University, No. 72 Xiangya Road, Changsha 410000, Hunan, China

² Department of Hematology/Molecular Biology Research Center, Center for Medical Genetics, School of Life Sciences/Hunan Province Key Laboratory of Basic and Applied Hematology, The Second Xiangya Hospital of Central South University, Central South University, No. 72 Xiangya Road, Changsha 410011, China



to their enhanced modifiability, optimized development, and production efficiency, and reduced risk of insertional mutations compared to conventional peptide vaccines [8, 9]. Although human papillomavirus (HPV) vaccines were shown to contribute to cervical cancer prevention, their effect on cancer incidence may be limited due to the slow development of precancerous lesions [10, 11]. This limitation underscores the need for vaccines stimulating cell-mediated immune responses to effectively target and eliminate infected cells [12]. Moreover, a significant proportion of patients with cervical cancer are HPV-negative, emphasizing the necessity for alternative therapeutic approaches [13].

Recently, the dynamic landscape of regulated cell death mechanisms, specifically ferroptosis and cuproptosis, has garnered increasing attention in the context of cancer biology and precision treatment [14–16]. First proposed by Stockwell et al., ferroptosis is characterized by iron-dependent lipid peroxidation [17, 18]. Cuproptosis, a more recently identified form of cell death, is induced by copper targeting fatty acylated TCA cycle proteins [19]. Both iron (Fe) and copper (Cu), essential trace elements for living organisms [20], play crucial roles in cuproptosis and ferroptosis. Intriguingly, copper ions can affect iron metabolism [21], and excessive copper accumulation potentially exacerbates iron-mediated toxicity and oxidative stress [22]. Moreover, the degradation of ATP7A, a key copper transmembrane transporter, has been linked to increased levels of reactive oxygen species (ROS) and ferroptosis [23]. Several bioinformatics analyses have revealed the associations between cuproptosis-related genes (CRGs) and ferroptosis-related genes (FRGs), leading to the establishment of prognostic models in various cancers [24–28]. However, the specific interplay between cuproptosis and ferroptosis and its clinical significance in cervical cancer remains unexplored.

This study aimed to address these knowledge gaps by comprehensively exploring cuproptosis–ferroptosis interaction in cervical cancer. We sought to elucidate the molecular mechanisms underlying the cross-talk between these two cell death pathways and identify cervical cancer subtypes associated with distinct cuproptosis and ferroptosis patterns. By developing a novel prognostic gene signature based on the cuproptosis–ferroptosis interactome, we aimed to deepen our understanding of cervical cancer progression and improve patient stratification. Furthermore, we explored the potential of these identified subtypes and gene signatures in guiding the development of mRNA vaccine, potentially opening new avenues for personalized immunotherapy in cervical cancer.

To achieve these objectives, we comprehensively analyzed gene expression profiles of CRGs and FRGs

and constructed molecular interaction networks to identify the molecular subtypes of cervical cancer. We also applied machine learning algorithms to identify hub genes. By integrating clinical data, we evaluated the prognostic and biological significance of our findings and their potential therapeutic implications. Unraveling the complex interactions between cuproptosis and ferroptosis in cancer can improve the efficacy of existing treatments and guide the development of innovative treatment modalities, finally improving patients' outcomes.

Materials and methods

Data collection and processing

We obtained gene expression data and corresponding clinical information for 306 cervical squamous cell carcinoma and endocervical adenocarcinoma (CESC) samples from The Cancer Genome Atlas (TCGA) via the UCSC Xena database (<https://xena.ucsc.edu/>). This data set also included transcriptome data from ten normal cervical tissue samples from the GETx portal. After excluding patients with missing follow-up information or survival times of less than 1 month, 283 patients with CESC remained for survival analysis. The gene expression profile, measured by RNA sequencing, was normalized using the $\log_2(x + 1)$ transformed TPM (transcripts per million) values. We acquired an independent gene expression dataset (GSE44001) from the Gene Expression Omnibus (GEO) database (<https://www.ncbi.nlm.nih.gov/geo/>) for external validation. CFRGs were curated from published literature, resulting in a comprehensive list of 293 candidate genes [19, 26, 29] (Table S1).

Screening and analysis of key CFRGs

Correlation analysis

We employed the Spearman correlation method to determine the associations between CFRGs. Genes with $|\text{correlation coefficients}| > 0.3$ and adjusted p -value < 0.001 were selected for further analyses.

Differential expression analysis

Differential expression analysis of CFRGs was conducted using the limma package [30], with a threshold of $|\log_2\text{Foldchange}| > 1$ and an adjusted p -value < 0.05 . We also conducted a parallel analysis using raw count data processed with the DESeq2 method to ensure the robustness of differentially expressed genes (DEGs). Interestingly, Spearman correlation analysis revealed that the DEGs identified using Limma (using log TPM) and DESeq2 (using raw counts) were strongly correlated (correlation coefficient = 0.96, $P < 2.2e-16$) (Additional file: Fig. S1, Table S2).

Protein–protein interaction (PPI) network analysis

We used the STRING database to construct a PPI network for the 98 identified CFRGs. The network was visualized using Cytoscape software. In addition, we conducted an enrichment analysis of Wiki pathways for the identified CFRGs to unravel their biological significance.

Prognostic analysis and mutation analysis

We applied the univariate Cox regression algorithm to identify key CFRGs with prognostic significance in cervical cancer. In addition, the maftools package [31] was adopted to measure the mutation frequencies of these CFRGs.

Unsupervised clustering based on CFRGs and enrichment analysis

We employed the ConsensusClusterPlus package [32] to categorize patients with CESC into two distinct subtypes based on the expression levels of CFRGs. The clustering algorithm parameters were set as cluster-*Alg* = “km” and *distance* = “euclidean”. Validation of the distinct subtype distribution was conducted using principal component analysis (PCA). Kaplan–Meier (KM) curves were then employed to compare survival advantages between the identified subtypes. In addition, the clusterProfiler package [33] was employed to conduct gene ontology (GO) and gene set enrichment analysis (GSEA) and determine functional annotations associated with these subtypes.

Gene selection based on machine learning and signature construction**Machine learning-based gene selection**

Three common algorithms, namely, LASSO, XGBoost, and SVM–RFE, were employed to identify key CFRGs. For the LASSO method, we conducted tenfold cross-validation and set the penalty coefficient of each gene to 1. For the XGBoost method, we set the maximum depth of each tree to 6 and chose the “gain” parameter to represent the importance of CFRG. For the SVM–RFE method, we estimated an internal tenfold CV error at each combination of SVM hyperparameters (*Cost* and *Gamma*) using grid search.

Prognostic signature construction and evaluation

We used a Cox proportional hazards model to establish a 4-gene signature for predicting the prognosis of patients with CESC. The risk score for each patient was calculated using the following formula:

$$\text{Riskscore} = \sum_{(i=1)}^n \text{Coef}_i \times \text{Exp}_i,$$

Patients with CESC were stratified into high-risk or low-risk groups based on the median risk score of the 4-gene signature. The receiver operating characteristic (ROC) curve was adopted to calculate the area under the curve (AUC) values for 1 year, 3 year, and 5 year overall survival (OS). In addition, univariate and multivariate Cox analyses were conducted to determine the independent factors associated with risk scores and other clinical features.

Analysis of the tumor microenvironment, response to immunotherapy, and anti-tumor drug susceptibility

We utilized the ESTIMATE package [34] for patients with CESC to comprehensively analyze the tumor microenvironment (TME), including immune and stromal components, and the overall TME score. Furthermore, employing the CIBERSORT algorithm [35], we assessed the infiltration of 22 immune cell types. Tumor immune dysfunction and exclusion (TIDE) tool [36] was used to estimate TIDE scores and predict response to immunotherapy in patients with CESC. Subsequently, using the oncoPredict package [37], we calculated the sensitivity to 198 anti-tumor drugs using pharmacogenomic data from the Genomics of Drug Sensitivity in Cancer (GDSC) 2 database as the training dataset.

Reverse transcription quantitative polymerase chain reaction (RT-qPCR)

For experimental validation, we collected 16 tumor samples and 5 adjacent normal tissue samples after surgical resection at the Second Xiangya Hospital of Central South University between January 2023 and June 2023. Fresh tissue specimens were immediately snap-frozen in liquid nitrogen after surgical removal and stored at -80°C until RNA extraction. The RT-qPCR procedure was conducted following our previously described methodology [38, 39]. Following tissue homogenization, Trizol lysis buffer was utilized to extract total RNA. Thereafter, reverse transcription was conducted to generate cDNA. A preliminary assessment of experimental test reaction efficiency yielded a range of 95 to 105%. A single peak in the melting curve signifies the primer's specificity. Ct values were experimentally derived and processed using the standard $2^{-\Delta\Delta\text{Ct}}$ method. Primers specific to the 4-gene panel were designed as follows:

TSC22D3:

Forward Primer: GGATGAACAAGGGGATGGCT

Reverse Primer: ACCCGCTACAGACAAGCTTT

SQLE:

Forward Primer: GATGATGCAGCTATTTTC

GAGGC

Reverse Primer: CCTGAGCAAGGATATTCACGACA
TFRC:

Forward Primer: AAAATCCGGTGTAGGCACAG

Reverse Primer: TTAAATGCAGGGACGAAAGG

ZNF419:

Forward Primer: GCTATGTGACCTTTGAGGATGT

Reverse Primer: CAGAGAGGCCAGAAGTGTAAG

Statistical analysis

All statistical analyses and visualizations were conducted using R software (version 4.2.3) and GraphPad Prism software (version 8.0.1). Differences between different subgroups were assessed using student's *t*-test unless otherwise specified. The log-rank test was employed to calculate *p*-values in Kaplan–Meier curves. All *p*-values were two-sided, and statistical significance was defined as $P < 0.05$ unless explicitly stated otherwise.

Results

Characterization of CFRGs in CESC

We first analyzed the correlation of CRGs with FRGs using the Spearman method to identify potential CFRGs. In total, 221 candidate CFRGs were visualized using ggalluvial package (Fig. 1A). PPI network analysis revealed significant interactions among the 221 CFRGs (p -value $< 1.0e-16$) (Fig. 1B). Functional enrichment of the network showed involvement in biological processes, such as copper metabolism and ferroptosis, highlighting the interaction between cuproptosis and ferroptosis (Fig. 1C). Next, we identified 98 differentially expressed CFRGs between normal tissues and tumors (Fig. 1D, Table S3). Univariate Cox regression analysis also identified 17 CFRGs with prognostic significance (Fig. 1E). The mutation frequencies of these 17 prognostic CFRGs were generally low among patients with CESC (overall mutation frequency: 9.34%), evidenced by the waterfall plot (Fig. 1F).

Two distinct subtypes of CFRGs-related CESC

Cervical cancer exhibits substantial molecular heterogeneity, and recent studies have identified distinct molecular subtypes associated with different prognoses and potential therapeutic implications [40–42]. For example, a transcriptomic study identified four distinct subtypes, including hypoxia, proliferation, differentiation,

and immune activity. These subtypes are characterized by specific genetic and epigenetic alterations and differential expression of key genes and pathways. We identified two stable and distinct CFRG-related CESC subtypes using consensus clustering (Figs. 2A, B). The PCA algorithm confirmed that Cluster 1 and Cluster 2 had different distributions (Fig. 2C). The subtypes exhibited distinct expression patterns of CFRGs (Fig. 2D). In particular, Cluster 2 was associated with significantly favorable survival compared to Cluster 1 (Fig. 2E). Gene ontology enrichment of DEGs between subtypes implicated immune-related pathways, such as humoral immune response and complement activation (Fig. 2F). GSEA showed that oncogenic pathways were significantly enriched in Cluster 1 (Fig. 2G). These results suggest that CFRG expression patterns may be associated with differences in survival outcomes and immune-related processes in CESC, although further validation is needed to confirm these findings.

Screening key CFRGs with prognostic values based on machine learning

We applied several machine learning techniques for feature selection to identify key CFRGs that can predict prognosis. First, the LASSO method identified 13 optimal gene combinations with the minimum partial likelihood deviation (Fig. 3A). Next, the XGBoost algorithm ranked CFRGs based on their relative importance, from which we selected the top 10 candidates (Fig. 3B). Meanwhile, the SVM–RFE was used to generate error curves, indicating that the optimal number of features was 9 (Fig. 3C). By intersecting the candidate genes obtained from LASSO, XGBoost, and SVM–RFE, we identified four CFRGs, including TSC22D3, SQLE, ZNF419, and TFRC, as the most important predictors of prognosis (Fig. 3D).

Generation of a CFRGs-related signature

Building upon the four identified CFRGs, we established a prognostic signature for patients with CESC using the Cox proportional hazards model. The risk score was calculated as follows: Risk score = $(-0.276) * TSC22D3 + 0.237 * SQLE + 0.360 * ZNF419 + 0.216 * TFRC$. KM curves indicated that patients in the high-risk group had significantly worse OS compared to those

(See figure on next page.)

Fig. 1 Identification and characterization of CFRGs in CESC. **A** A total of 211 genes significantly correlated between FRGs and CRGs. Due to the extensive number of FRGs, the specific FRGs are not listed in the legend. **B** STRING database revealed PPI network among the 211 CFRGs. **C** The enrichment strength of the PPI network in WIKI pathway platform. FDR: false discovery rate. **D** The volcano plot showed differentially expressed CFRGs in CESC. **E** Univariate Cox regression analysis identifying 17 CFRGs significantly associated with CESC patient prognosis. **F** Mutation frequency of the 17 prognostic CFRGs across cervical cancer patients from TCGA cohort. * $p < 0.05$, ** $p < 0.01$

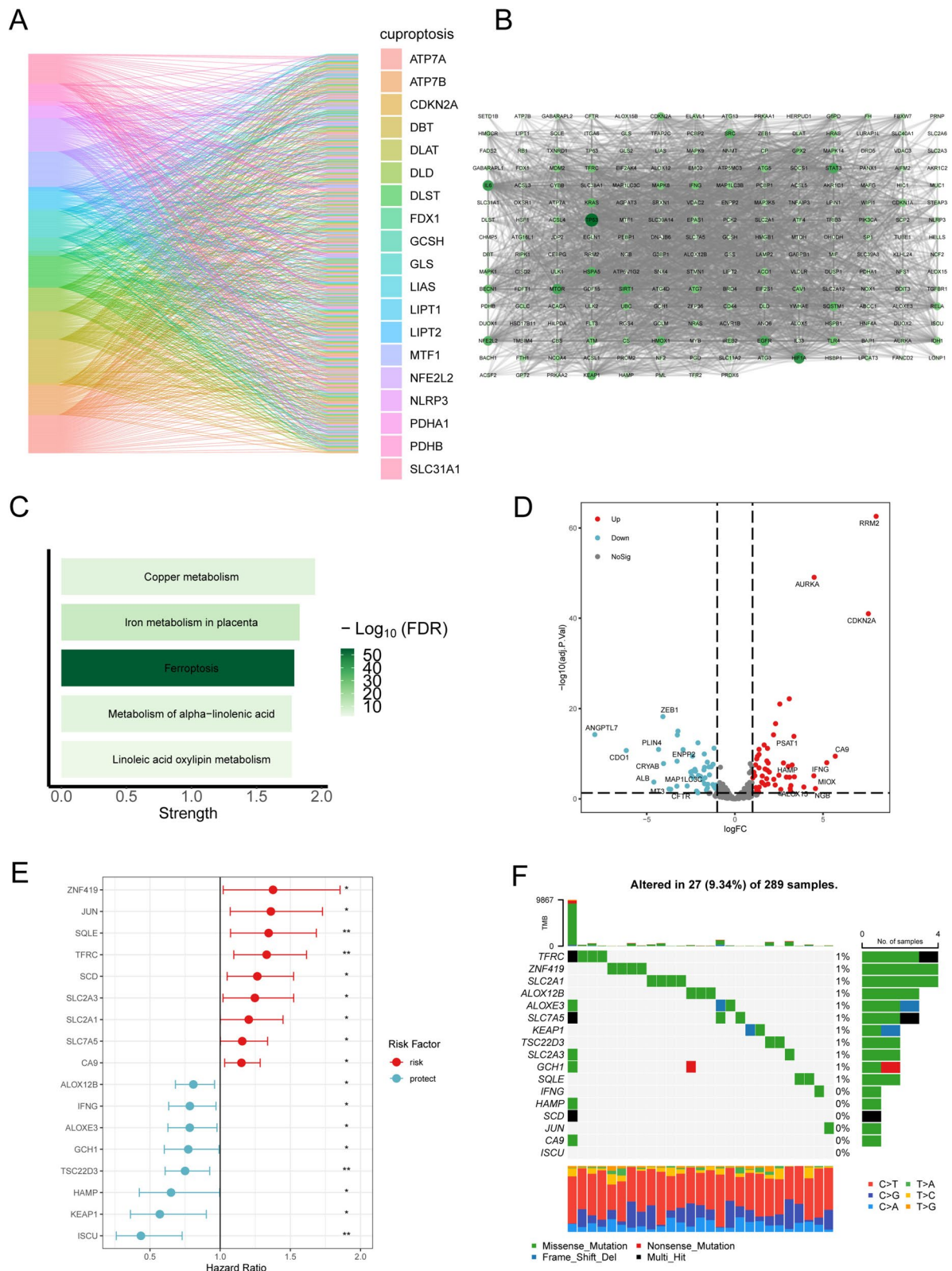


Fig. 1 (See legend on previous page.)

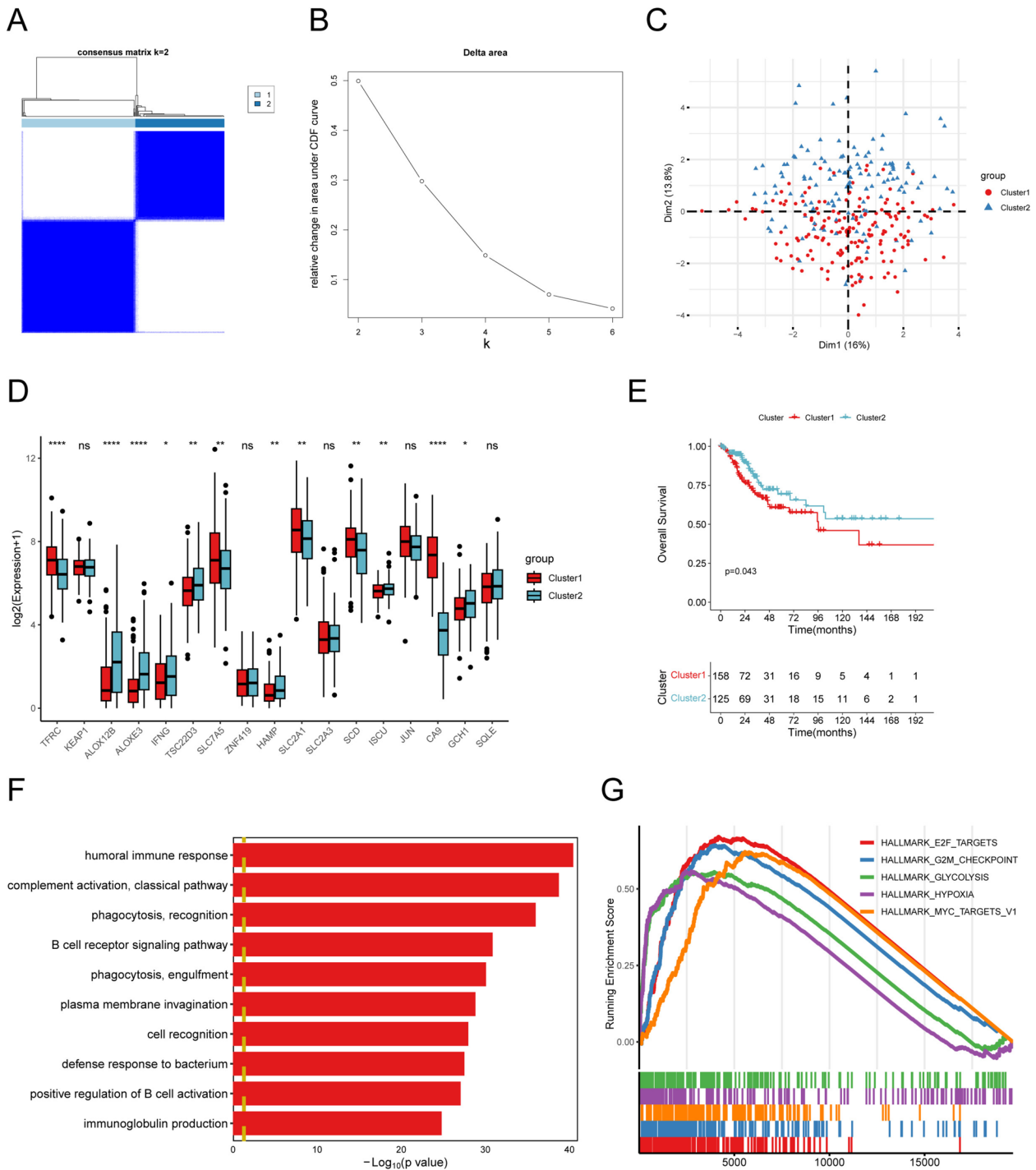


Fig. 2 CFRGs-related molecular subtypes of CESC patients. **A** Consensus heatmap of the two subtypes when $k=2$. **B** The relative change of cumulative distribution function (CDF) curves when $k=2-6$. **C** PCA plot showed separation of the two subtypes based on the 17 prognostic CFRGs expression. **D** Comparative analysis of expression levels for the 17 CFRGs between the two CESC subclusters. **E** KM analysis implemented to compare OS probabilities between the identified CESC subtypes. **F** Enrichment analysis highlighting the top ten GO terms associated with DEGs. **G** The top five hallmark gene sets ranked by GSEA algorithm. * $p < 0.05$, ** $p < 0.01$, *** $p < 0.001$, **** $p < 0.0001$

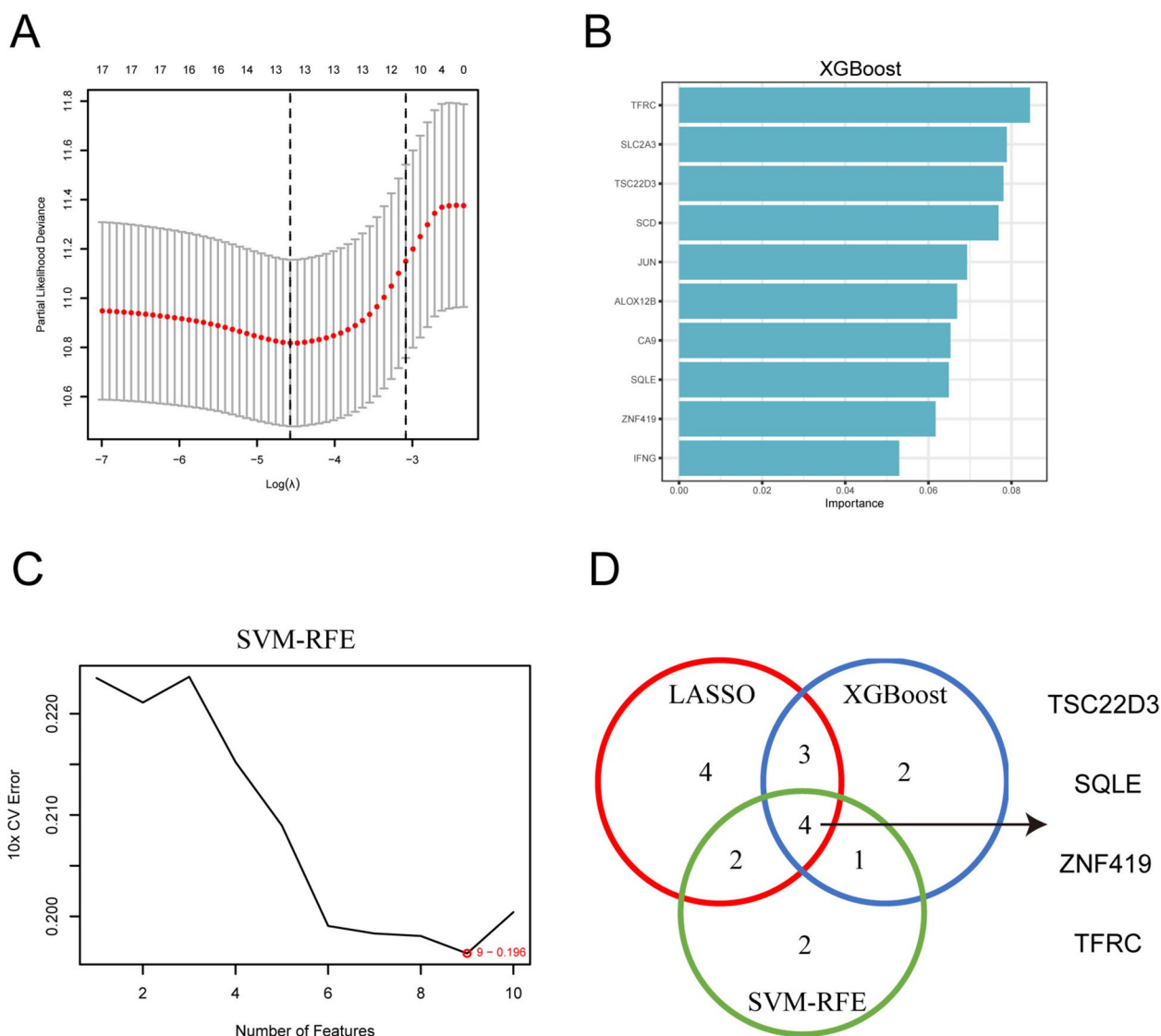


Fig. 3 Identification of critical prognostic CFRGs using machine learning algorithms. **A** Distribution of partial likelihood deviance for log (λ) in LASSO regression, illustrating the regularization path. **B** Feature importance obtained through XGBoost, highlighting key contributors to prognoses of CESC patients. **C** Distribution curve depicting the relationship between the number of features and tenfold cross-validation error. **D** Venn diagram revealed 4 key CFRGs

in the low-risk group ($p=0.0011$) (Fig. 4A). The ROC analysis yielded AUC values of 0.78, 0.67, and 0.67 for 1 year, 3 year, and 5 year OS, respectively, suggesting moderate prognostic ability (Fig. 4B). Validation in an external cohort also confirmed the predictive power of the 4-gene signature (Fig. 4C). Univariate and multivariate Cox regression incorporating clinical covariates revealed that the 4-gene signature could serve as an independent prognostic factor for OS (univariate: HR=1.652, $p<0.001$; multivariate: HR=1.735, $p=0.027$) (Fig. 4D, E). Stratification analyses showed that the signature stratified patients' risk across age and stage

(Fig. 4F, G), exhibiting robust performance in different clinical contexts. Together, these findings suggest that this 4-gene signature may possess potential prognostic value in CESC.

Analysis of tumor microenvironment infiltration

Ferroptosis or cuproptosis has been previously documented to interact with the tumor microenvironment (TME) and modulate anti-tumor immune responses [43]. This study revealed a significant enrichment of DEGs associated with CFRGs in immune-related functions (Fig. 2F).

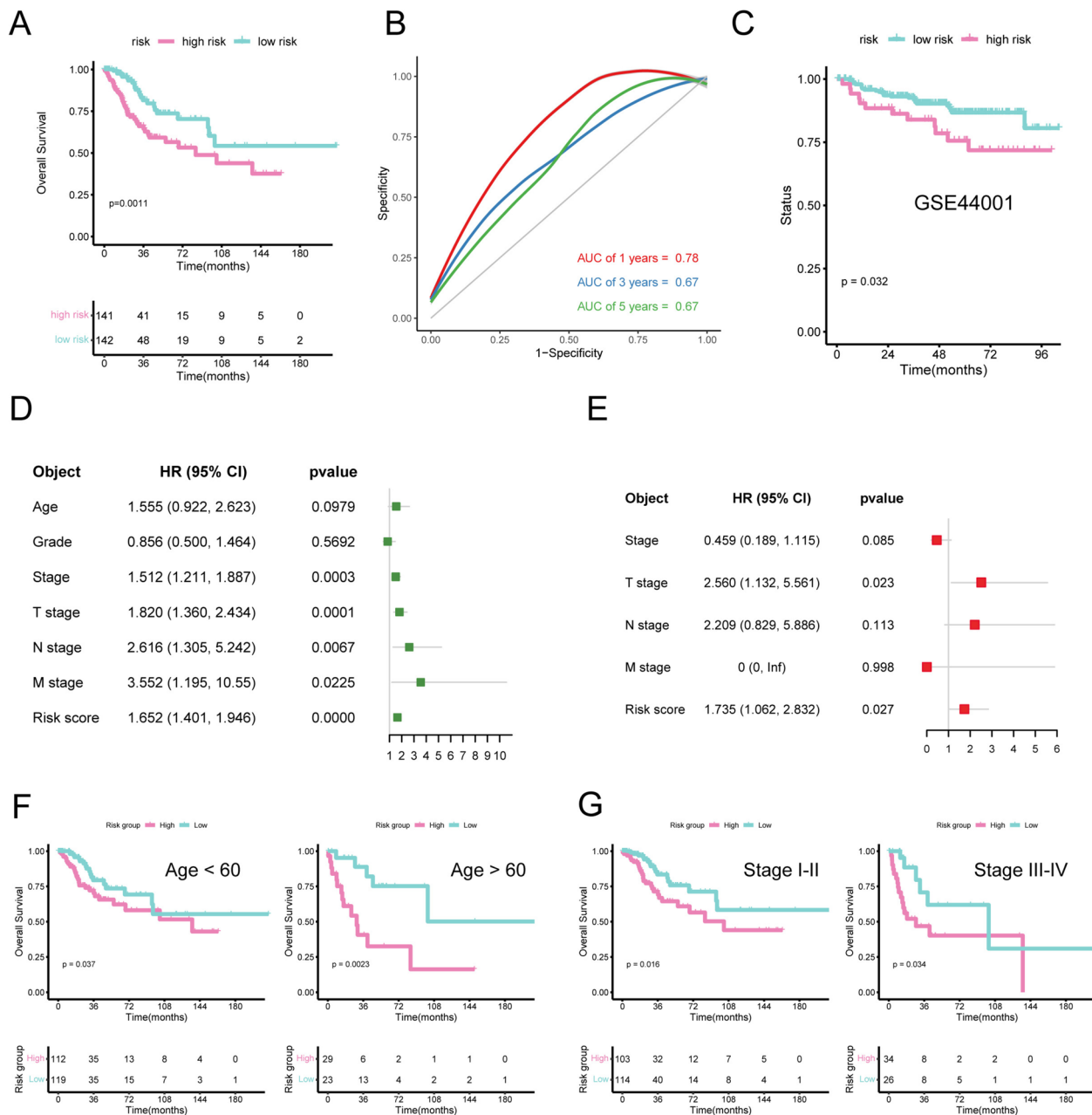


Fig. 4 Construction and validation of a CFRGs-related 4-gene signature in CESC. **A** The low-risk patients had prominent OS advantage compared with high-risk ($p=0.0011$, log-rank test). **B** Time-dependent ROC curves showing AUC values of 0.78, 0.67 and 0.67 for 1-, 3- and 5 year OS prediction, respectively. **C** Independent validation of our signature in GEO cohorts (GSE44001). **D, E** Univariate and multivariate Cox analyses of the 4-gene signature alongside other clinicopathological variables. **F, G** The application of 4-gene signature under clinical stratification

(See figure on next page.)

Fig. 5 Characterization of TME patterns in prognostic subgroups. **A** Boxplots showing significantly higher immune and ESTIMATE scores, measuring immune infiltration, in the low-risk group (Mann–Whitney U test) **B** Scatter plot revealing significant negative correlations between risk scores and immune as well as ESTIMATE scores. **C** The expression of immune checkpoint genes between subgroups, with upregulation in low-risk. **D** The low-risk patients had higher cytotoxicity scores. **E** The TME pattern in the two subgroups. **F** 7 cell types were identified based on canonical markers in GSE168152. **G** The violin plot illustrating the 4-gene signature scores across different cell types. * $p < 0.05$, ** $p < 0.01$, *** $p < 0.001$, **** $p < 0.0001$

Therefore, we assessed TME infiltration levels in two distinct risk groups of patients. Utilizing the ESTIMATE algorithm, our analysis revealed that low-risk patients have elevated immune and ESTIMATE scores (Fig. 5A). The scatter plot also confirmed a negative correlation between risk scores and both immune and ESTIMATE scores (Fig. 5B). In addition, we observed high expression levels of immune checkpoint genes in the low-risk patient group (Fig. 5C). Calculation of cytotoxicity scores indicated that low-risk patients exhibit high anti-tumor activity (Fig. 5D). Furthermore, a comparative analysis of the proportions of 22 types of lymphocytes indicated differences between the two risk groups, particularly in five distinct cell types (Fig. 5E). For instance, the high-risk group exhibited a lower abundance of CD8+T cells and a higher abundance of M0 macrophages. We employed the CESC dataset GSE168652 from the TISCH database to enhance the accuracy of our analysis of the 4-gene signature in the TME [44]. Based on canonical markers, we identified seven cell types, including CD8+T cells, endometrial stromal cells, endothelial cells, fibroblasts, malignant cells, monocytes/macrophages, and smooth muscle cells (Fig. 5F). The violin plot suggested that the 4-gene signature had the highest scores in CD8+T cells, malignant cells, and Mono/Macro cells, confirming the findings from bulk RNA-seq data (Fig. 5G).

RNA N6-methyladenosine (m6A) plays a pivotal role in remodeling the TME in different types of cancer and other diseases [45, 46]. Therefore, we compared the expression levels of 23 m6A regulators between the two risk groups. Boxplot analysis revealed a substantial increase in nearly all m6A regulators in the high-risk group (Additional file: Fig. S2). Collectively, these results support the interaction between ferroptosis/cuproptosis and tumor immunity.

Single-nucleotide variation (SNV) and response to immunotherapy

We analyzed mutation profiles between the high-risk and low-risk groups. The top five most frequently mutated genes in the high-risk group were PIK3CA, TTN, MUC16, FLG, and SYNE1 (Fig. 6A). Meanwhile, the top five most frequently mutated genes in the low-risk group were TTN, PIK3CA, KMT2C, MUC16, and DMD (Fig. 6B). Subsequently, we computed the tumor mutational burden (TMB) for each patient with CESC. Correlation analysis revealed a significant positive correlation between the risk score and TMB (Fig. 6C). Further comparative analysis of mutated genes revealed that high-risk patients had higher mutation

frequencies in multiple genes, such as BRCA2, and TP53 (Fig. 6D). We applied the TIDE algorithm to assess the efficacy of immunotherapy among patients with CESC. The results indicated that high-risk patients possessed high TIDE scores (Fig. 6E). Moreover, the barplot indicated that low-risk patients were more likely to benefit from immunotherapy (Fig. 6F). These results suggest differences in mutation patterns and predicted immunotherapy response between the risk groups.

Prediction of response to anti-tumor drugs

To advance personalized treatment, we investigated differences in predicted response to anti-tumor drugs between prognostic subgroups. Sensitivity comparison and correlation analyses unveiled that the top 5 most effective drugs for low-risk patients were AZD6482, ribociclib, PF.4708671, KU.55933, and topotecan (Figs. 7A, B). Conversely, high-risk patients showed the best response to BI.2536, linsitinib, UMI.77, osimertinib, and NVP.AD742 (Figs. 7C, D). These results provided insight into differential treatment strategies for CESC based on the risk defined using the CFRG signature. Targeting pathways modulated by sensitive drugs may improve clinical outcomes for each subgroup of patients.

RT-qPCR

We collected 16 tumor samples and 5 para-carcinoma samples from patients with cervical cancer to validate the expression of the identified 4-gene signature. After collection, we conducted qRT-PCR experiments on these samples to assess the expression levels of TSC22D3, SQLE, ZNF419, and TFRC. Compared to normal adjacent tissues, SQLE and TFRC were upregulated in tumor tissues, whereas TSC22D3 and ZNF419 were downregulated (Fig. 8A, B). Notably, our results for SQLE and TFRC align with the results of previous studies demonstrating significant upregulation of these genes in cervical cancer [47, 48]. Interestingly, changes in ZNF419 expression in our experiments were inconsistent with its coefficient in the risk score model. This phenomenon is not unprecedented in cancer research. Our risk score was developed using a machine learning approach that integrates expression patterns from several genes to provide a composite risk metric. Similar inconsistencies have been reported in previous studies on cervical cancer and other types of cancer [49–51]. To address this discrepancy and validate our findings, we recognize the need for additional analyses in independent cohorts. Future studies are crucial to evaluate the performance and robustness of our risk score model across different settings.

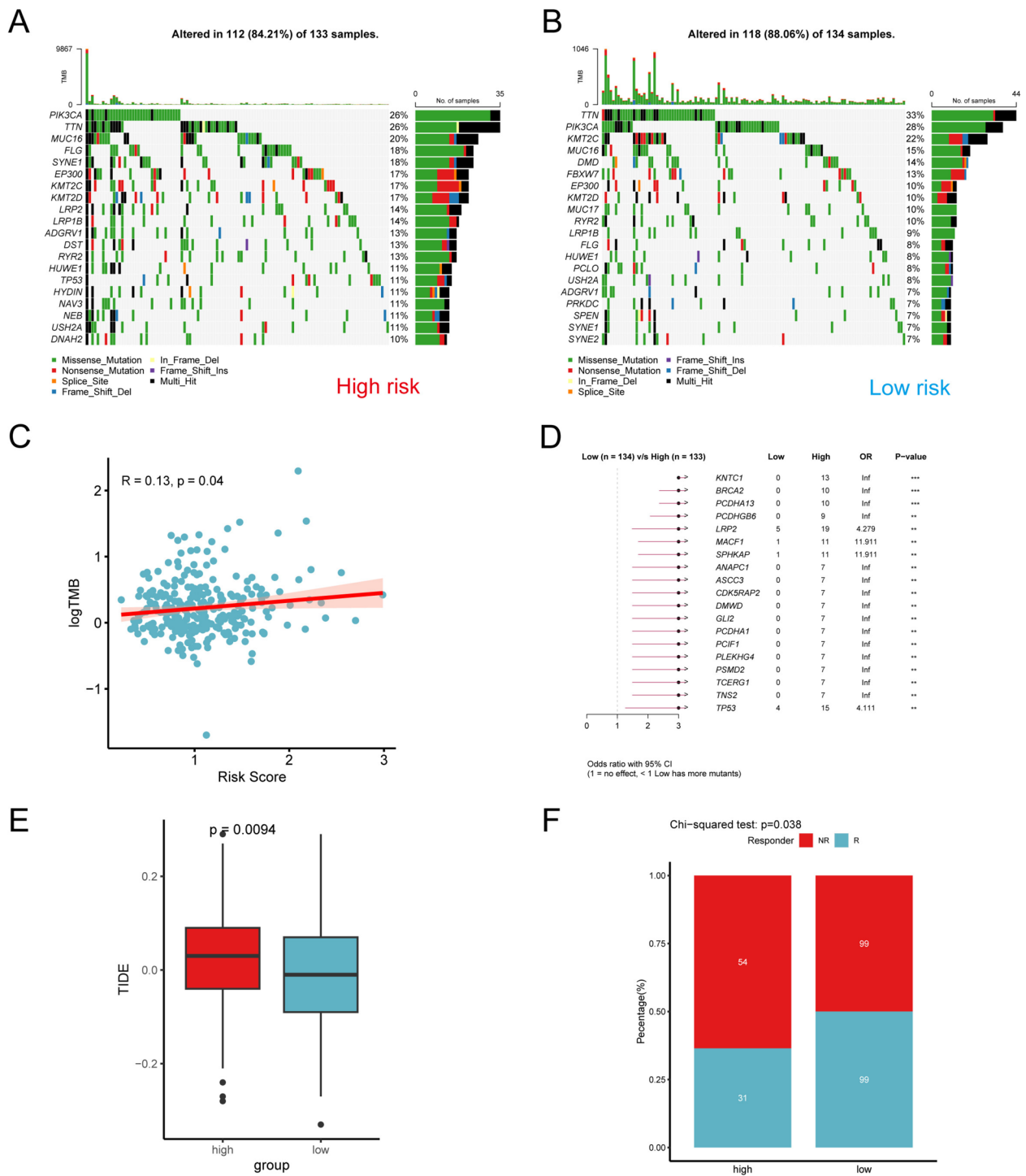


Fig. 6 Tumor mutation burden and immunotherapy analysis. **A, B** The top 20 genes with the highest mutation frequency in the high-risk (**A**) and low-risk subgroups (**B**). **C** Positive correlation observed by the risk score with TMB (Spearman method). **D** Comparison of significantly different mutated genes between high-risk and low-risk subgroups. **E** TIDE score comparison between the two risk subgroups, indicating potential response to immunotherapy. **F** Stacked bar plot illustrating a higher response rate to immunotherapy in the low-risk group. ** $p < 0.01$, *** $p < 0.001$

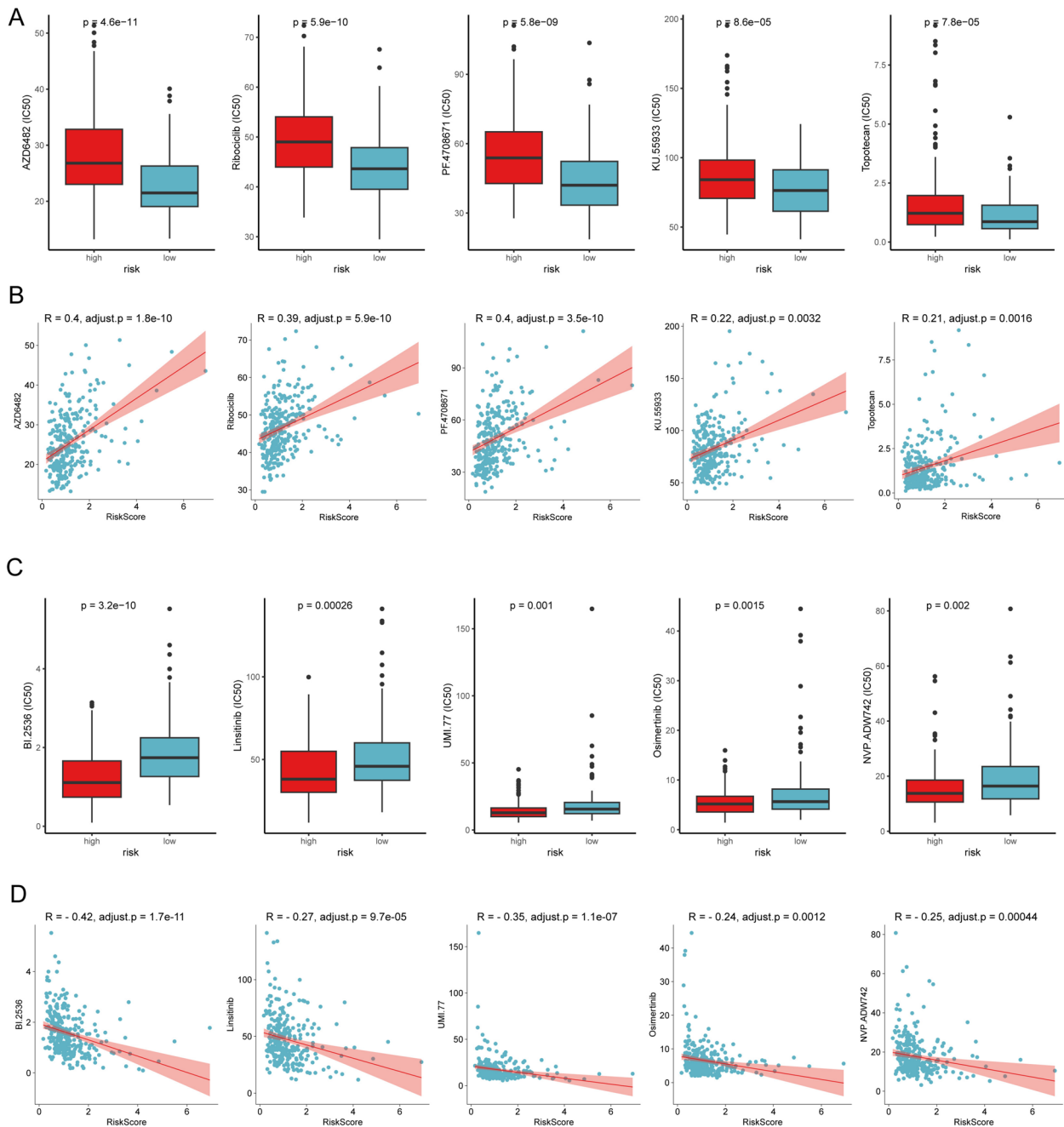


Fig. 7 Predicted sensitivity to anti-tumor drugs between prognostic subgroups. **A, C** Boxplots depicting the differences in the top 5 drug sensitivities between the two risk subtypes. **B, D** Correlation scatter plots illustrating the significant associations between drug sensitivity and the risk score in the TCGA-CESC cohort

Discussion

This study unraveled the intricate interplay between cuproptosis and ferroptosis in cervical cancer. Studies on regulated cell death mechanisms, specifically ferroptosis and cuproptosis, have increasingly gained attention in the context of cancer biology and precision treatment [43, 52]. Therefore, it is very necessary to study the effect of

ferroptosis and cuproptosis on signal transduction, prognosis, and pharmacological treatment in cervical cancer.

Our analysis revealed the enrichment of CFRGs in copper and iron metabolism, highlighting their importance in homeostatic regulation through intricate copper-iron interactions. Previous reports supported this conclusion, demonstrating that copper facilitates ferroptosis

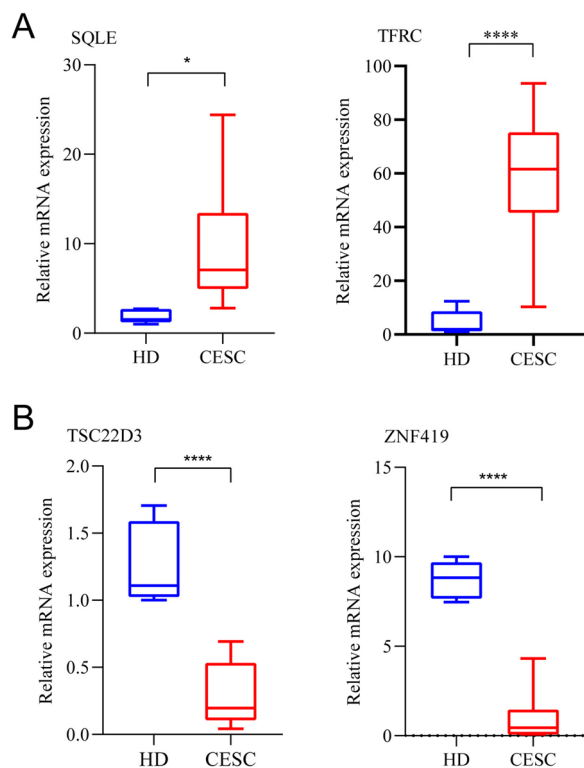


Fig. 8 Experimental validation of the 4-gene signature by RT-qPCR. **A, B** Cervical cancer tumor tissues ($n=16$) compared to adjacent normal tissues ($n=5$) obtained from patients at the Second Xiangya Hospital. HD: Healthy Donors. * $p < 0.05$, **** $p < 0.0001$

by degrading the key inhibitor of ferroptosis GPX4 [53]. Copper chelators can reduce the sensitivity to ferroptosis, without inhibiting other forms of cell death. Controlling copper-iron homeostasis in malignant tumors and promoting cell death are interesting therapeutic strategies.

Currently, mRNA technology stands as a principal approach in the development of tumor vaccines. Numerous studies have documented the use of mRNA vaccines in the treatment of cancer, presenting promising therapeutic possibilities for personalized interventions [54–56]. However, the clinical advantages observed among patients receiving mRNA-based vaccines remain limited to specific groups. This study delineated two subtypes associated with CFRGs, each possessing unique molecular, immunological, and clinical characteristics. Our findings offer invaluable insights into the application of tumor vaccines.

Although the close link between ferroptosis and cervical cancer has been previously reported [57], ferroptosis and cuproptosis were not shown to reshape the immune microenvironment and regulate the anti-tumor immune response in cervical cancer. This study highlighted the importance of CFRGs in regulating immune responses

and the TME. Considering that immunotherapy is gradually being incorporated into the treatment of cervical cancer [58], the identification of novel biomarkers or the combined use of cuproptosis or/and ferroptosis inducers is a promising strategy for cancer immunotherapy.

Using machine learning methods, we identified a 4-gene signature (TSC22D3, SQLE, ZNF419, and TFRC) with significant prognostic relevance. TSC22D3 is a ferroptosis marker gene [59]. A previous bioinformatics study also identified TSC22D3 as a prognostic marker for gynecological cancer [60]. This consistency showed the potential of TSC22D3 in predicting the prognosis of patients with cervical cancer. SQLE, implicated in the CoQ10 pathway, acts as a defense mechanism against ferroptosis by inhibiting the generation of reactive oxygen species (ROS) [61]. Moreover, SQLE was shown to be associated with cuproptosis [62]. Guo et al. found that SQLE is highly expressed in patient tissues and several cervical cancer cell lines [47]. SQLE regulates the proliferation, migration, and invasion of CC cells by inactivating the p53 pathway. Interestingly, we found a higher frequency of TP53 mutations in the high-risk group (Fig. 6D). The specific mechanism of SQLE and TP53 signaling pathway is a topic worthy of further studies. ZNF219 is involved in the activation of p53, which subsequently modulates both ferroptosis and cuproptosis [63, 64]. There is still a lack of research on ZNF219 in cervical cancer. However, a bioinformatics study suggested that ZNF419 can serve as a pan-cancer biomarker [65]. Transferrin receptor (TFRC) is a key driver of ferroptosis [66]. Huang et al. found that after TFRC knockdown, cervical cancer cells exhibited significant changes in various physiological processes, such as immune response and cell metabolism [67]. This addition, two studies have shown that propofol or hyperoside can inhibit cervical cancer cell growth by regulating TFRC, showing therapeutic promise [68, 69]. Collectively, these studies support the potential of the 4-gene signature for tumor development, prognosis, and therapeutic applications in cervical cancer.

This study significantly advances the current understanding of CESC. Firstly, we identified a novel 4-gene signature (TSC22D3, SQLE, ZNF419, and TFRC) with prognostic value in CESC. This signature was obtained through a rigorous process involving multiple machine learning algorithms (LASSO, XGBoost, and SVM-RFE) and can improve clinical decision-making and personalized treatment strategies. In addition, our unsupervised clustering analysis revealed two distinct CESC subtypes based on CFRG expression profiles. These subtypes showed significant differences in terms of survival and were associated with distinct biological processes. This finding provides new insights into the heterogeneity of

CESC and can guide future research on targeted treatment. Finally, our integrative analysis of gene expression, mutation data, and PPI has expanded our understanding of the complex interplay between cuproptosis and ferroptosis in CESC. This comprehensive approach highlighted potential mechanisms underlying the progression of CESC and identified novel therapeutic targets.

Despite the use of multi-omics datasets, This study had certain limitations. The discrepancy observed in ZNF419 expression between our experimental results and the risk score model should be addressed in future studies in independent cohorts. This addition, the functional roles of the genes in our signature, particularly in the context of cuproptosis and ferroptosis, should be explored through *in vitro* and *in vivo* experiments. Moreover, mechanistic studies elucidating the associations between CFRGs and the immune context are needed. Finally, larger multicenter prospective cohorts are needed to validate the prognostic value of the 4-gene signature.

In conclusion, this study introduced a novel perspective on CESC biology through the lens of cuproptosis and ferroptosis, offering potential prognostic tools and new targets for treatment.

Conclusion

Our comprehensive study established a novel 4-gene signature as a potent prognostic tool, offering invaluable insights for the personalized management of cervical cancer. By bridging the knowledge gaps toward cuproptosis, ferroptosis, and their interplay, this study contributes to the evolving landscape of cancer biology and introduces new targets for individualized therapeutic interventions. The identified genes, namely TSC22D3, SQLE, ZNF419, and TFRC hold promise not only as prognostic markers but also as potential antigens for developing future mRNA vaccines in cervical cancer.

Supplementary Information

The online version contains supplementary material available at <https://doi.org/10.1186/s40001-024-02191-x>.

Supplementary Material 1
Supplementary Material 2
Supplementary Material 3
Supplementary Material 4

Acknowledgements

We would like to express our gratitude to EditSprings (<https://www.editsprings.cn>) for the expert linguistic services provided.

Author contributions

W.Z. and H.G. contributed the idea for the article. X.Z., W.X., and Z.W. performed the experiments and analyzed the data. W.Z. and H.G. wrote the original manuscript. X.Z., W.X., Z.W., and J.L. revised the manuscript. All authors read and approved the final manuscript.

Funding

This study was funded by Postgraduate Scientific Research Innovation Project of Hunan Province (Grants number CX20220132).

Availability of data and material

No datasets were generated or analysed during the current study.

Declarations

Ethics approval and consent to participate

Ethical permissions were granted by the institutional review board of the Second Xiangya Hospital of Central South University (approval number: Z0667-01). All patients provided their informed written consent to participate in this study. The study was conducted in accordance with the Declaration of Helsinki.

Consent for publication

Not applicable.

Competing interests

The authors declare no competing interests.

Received: 21 January 2024 Accepted: 2 December 2024

Published online: 19 December 2024

References

- Sharma K, Machalek DA, Toh ZQ, Amenu D, Muchengeti M, Ndllovu AK, et al. No woman left behind: achieving cervical cancer elimination among women living with HIV. *Lancet HIV*. 2023;10(6):e412–20.
- Kromidas E, Geier A, Weghofer A, Liu HY, Weiss M, Loskill P. Immunocompetent PDMS-free organ-on-chip model of cervical cancer integrating patient-specific cervical fibroblasts and neutrophils. *Adv Healthc Mater*. 2023. <https://doi.org/10.1002/adhm.202302714>.
- Stockwell BR. Ferroptosis turns 10: emerging mechanisms, physiological functions, and therapeutic applications. *Cell*. 2022;185(14):2401–21.
- Wang M, Zheng L, Ma S, Lin R, Li J, Yang S. Cuproptosis: emerging biomarkers and potential therapeutics in cancers. *Front Oncol*. 2023;13:1288504.
- Nguyen TT, Wei S, Nguyen TH, Jo Y, Zhang Y, Park W, et al. Mitochondria-associated programmed cell death as a therapeutic target for age-related disease. *Exp Mol Med*. 2023;55(8):1595–619.
- Linares-Fernandez S, Lacroix C, Exposito JY, Verrier B. Tailoring mRNA vaccine to balance innate/adaptive immune response. *Trends Mol Med*. 2020;26(3):311–23.
- Saxena M, van der Burg SH, Melief CJM, Bhardwaj N. Therapeutic cancer vaccines. *Nat Rev Cancer*. 2021;21(6):360–78.
- Pardi N, Hogan MJ, Porter FW, Weissman D. mRNA vaccines—a new era in vaccinology. *Nat Rev Drug Discov*. 2018;17(4):261–79.
- Liu X, Huang P, Yang R, Deng H. mRNA cancer vaccines: construction and boosting strategies. *ACS Nano*. 2023;17(20):19550–80.
- Wang R, Pan W, Jin L, Huang W, Li Y, Wu D, et al. Human papillomavirus vaccine against cervical cancer: opportunity and challenge. *Cancer Lett*. 2020;471:88–102.
- Hancock G, Hellner K, Dorrell L. Therapeutic HPV vaccines. *Best Pract Res Clin Obstet Gynaecol*. 2018;47:59–72.
- Zhou P, Liu W, Cheng Y, Qian D. Nanoparticle-based applications for cervical cancer treatment in drug delivery, gene editing, and therapeutic cancer vaccines. *Wiley Interdiscip Rev Nanomed Nanobiotechnol*. 2021;13(5): e1718.
- Bhatla N, Aoki D, Sharma DN, Sankaranarayanan R. Cancer of the cervix uteri: 2021 update. *Int J Gynaecol Obstet*. 2021;155(Suppl 1):28–44.
- Mou Y, Wang J, Wu J, He D, Zhang C, Duan C, et al. Ferroptosis, a new form of cell death: opportunities and challenges in cancer. *J Hematol Oncol*. 2019;12(1):34.
- Zhao L, Zhou X, Xie F, Zhang L, Yan H, Huang J, et al. Ferroptosis in cancer and cancer immunotherapy. *Cancer Commun (Lond)*. 2022;42(2):88–116.

16. Chen L, Min J, Wang F. Copper homeostasis and cuproptosis in health and disease. *Signal Transduct Target Ther.* 2022;7(1):378.
17. Dixon SJ, Lemberg KM, Lamprecht MR, Skouta R, Zaitsev EM, Gleason CE, et al. Ferroptosis: an iron-dependent form of nonapoptotic cell death. *Cell.* 2012;149(5):1060–72.
18. Jiang X, Stockwell BR, Conrad M. Ferroptosis: mechanisms, biology and role in disease. *Nat Rev Mol Cell Biol.* 2021;22(4):266–82.
19. Tsvetkov P, Coy S, Petrova B, Dreishpoon M, Verma A, Abdusamad M, et al. Copper induces cell death by targeting lipoylated TCA cycle proteins. *Science.* 2022;375(6586):1254–61.
20. Grzeszczak K, Kwiatkowski S, Kosik-Bogacka D. The Role of Fe, Zn, and Cu in pregnancy. *Biomolecules.* 2020. <https://doi.org/10.3390/biom10081176>.
21. Festa RA, Thiele DJ. Copper: an essential metal in biology. *Curr Biol.* 2011;21(21):R877–83.
22. Klevay LM. IHD from copper deficiency: a unified theory. *Nutr Res Rev.* 2016;29(2):172–9.
23. Gao W, Huang Z, Duan J, Nice EC, Lin J, Huang C. Elesclomol induces copper-dependent ferroptosis in colorectal cancer cells via degradation of ATP7A. *Mol Oncol.* 2021;15(12):3527–44.
24. Xu L, Wang S, Zhang D, Wu Y, Shan J, Zhu H, et al. Machine learning- and WGCNA-mediated double analysis based on genes associated with disulfidptosis, cuproptosis and ferroptosis for the construction and validation of the prognostic model for breast cancer. *J Cancer Res Clin Oncol.* 2023;149(18):16511–23.
25. Luo G, Wang L, Zheng Z, Gao B, Lei C. Cuproptosis-related ferroptosis genes for predicting prognosis in kidney renal clear cell carcinoma. *Eur J Med Res.* 2023;28(1):176.
26. Shen Y, Li D, Liang Q, Yang M, Pan Y, Li H. Cross-talk between cuproptosis and ferroptosis regulators defines the tumor microenvironment for the prediction of prognosis and therapies in lung adenocarcinoma. *Front Immunol.* 2022;13:1029092.
27. Sun J, Guan C, Wang X, Zhu Z. A novel prognostic model between ferroptosis, cuproptosis, and disulfidptosis in predicting prognosis lung adenocarcinoma. *Asian J Surg.* 2024. <https://doi.org/10.1016/j.asjsur.2024.04.192>.
28. Zou Y, Xie J, Zheng S, Liu W, Tang Y, Tian W, et al. Leveraging diverse cell-death patterns to predict the prognosis and drug sensitivity of triple-negative breast cancer patients after surgery. *Int J Surg.* 2022;107: 106936.
29. Song J, Ren K, Zhang D, Lv X, Sun L, Deng Y, et al. A novel signature combining cuproptosis- and ferroptosis-related genes in sepsis-induced cardiomyopathy. *Front Genet.* 2023;14:1170737.
30. Ritchie ME, Phipson B, Wu D, Hu Y, Law CW, Shi W, et al. limma powers differential expression analyses for RNA-sequencing and microarray studies. *Nucl Acid Res.* 2015;43(7): e47.
31. Mayakonda A, Lin DC, Assenov Y, Plass C, Koeffler HP. Maftools: efficient and comprehensive analysis of somatic variants in cancer. *Genome Res.* 2018;28(11):1747–56.
32. Wilkerson MD, Hayes DN. ConsensusClusterPlus: a class discovery tool with confidence assessments and item tracking. *Bioinformatics.* 2010;26(12):1572–3.
33. Wu T, Hu E, Xu S, Chen M, Guo P, Dai Z, et al. ClusterProfiler 4.0: a universal enrichment tool for interpreting omics data. *Innovation (Camb).* 2021;2(3):100141.
34. Yoshihara K, Shahmoradgoli M, Martinez E, Vegesna R, Kim H, Torres-Garcia W, et al. Inferring tumour purity and stromal and immune cell admixture from expression data. *Nat Commun.* 2013;4:2612.
35. Newman AM, Liu CL, Green MR, Gentles AJ, Feng W, Xu Y, et al. Robust enumeration of cell subsets from tissue expression profiles. *Nat Method.* 2015;12(5):453–7.
36. Jiang P, Gu S, Pan D, Fu J, Sahu A, Hu X, et al. Signatures of T cell dysfunction and exclusion predict cancer immunotherapy response. *Nat Med.* 2018;24(10):1550–8.
37. Maeser D, Gruener RF, Huang RS. oncoPredict: an R package for predicting in vivo or cancer patient drug response and biomarkers from cell line screening data. *Brief Bioinform.* 2021. <https://doi.org/10.1093/bib/bbab260>.
38. Yang Q, Zhu W, Gong H. Subtype classification based on t cell proliferation-related regulator genes and risk model for predicting outcomes of lung adenocarcinoma. *Front Immunol.* 2023;14:1148483.
39. Gong H, Liu Z, Yuan C, Luo Y, Chen Y, Zhang J, et al. Identification of cuproptosis-related lncRNAs with the significance in prognosis and immunotherapy of oral squamous cell carcinoma. *Comput Biol Med.* 2024;171: 108198.
40. Burmeister CA, Khan SF, Schafer G, Mbatani N, Adams T, Moodley J, et al. Cervical cancer therapies: current challenges and future perspectives. *Tumour Virus Res.* 2022;13: 200238.
41. Li C, Wu H, Guo L, Liu D, Yang S, Li S, et al. Single-cell transcriptomics reveals cellular heterogeneity and molecular stratification of cervical cancer. *Commun Biol.* 2022;5(1):1208.
42. Yu L, Gao Z, Li Z, Liu P, Gao Y, Liang G. Identification of ferroptosis-related molecular subtypes and a methylation-related ferroptosis gene prognostic signature in cervical squamous cell carcinoma. *J Cancer Res Clin Oncol.* 2023;149(16):14673–89.
43. Tong X, Tang R, Xiao M, Xu J, Wang W, Zhang B, et al. Targeting cell death pathways for cancer therapy: recent developments in necroptosis, pyroptosis, ferroptosis, and cuproptosis research. *J Hematol Oncol.* 2022;15(1):174.
44. Sun D, Wang J, Han Y, Dong X, Ge J, Zheng R, et al. TISCH: a comprehensive web resource enabling interactive single-cell transcriptome visualization of tumor microenvironment. *Nucl Acid Res.* 2021;49(D1):D1420–30.
45. Mao Z, Wang B, Zhang T, Cui B. The roles of m6A methylation in cervical cancer: functions, molecular mechanisms, and clinical applications. *Cell Death Dis.* 2023;14(11):734.
46. Zhang X, Zhang S, Yan X, Shan Y, Liu L, Zhou J, et al. m6A regulator-mediated RNA methylation modification patterns are involved in immune microenvironment regulation of periodontitis. *J Cell Mol Med.* 2021;25(7):3634–45.
47. Guo M, Qiao Y, Lu Y, Zhu L, Zheng L. Squalene epoxidase facilitates cervical cancer progression by modulating tumor protein p53 signaling pathway. *J Obstet Gynaecol Res.* 2023;49(5):1383–92.
48. Song JY, Lee JK, Lee NW, Jung HH, Kim SH, Lee KW. Microarray analysis of normal cervix, carcinoma in situ, and invasive cervical cancer: identification of candidate genes in pathogenesis of invasion in cervical cancer. *Int J Gynecol Cancer.* 2008;18(5):1051–9.
49. Cai L, Hu C, Yu S, Liu L, Yu X, Chen J, et al. Identification and validation of a six-gene signature associated with glycolysis to predict the prognosis of patients with cervical cancer. *BMC Cancer.* 2020;20(1):1133.
50. Cai J, Hu Y, Ye Z, Ye L, Gao L, Wang Y, et al. Immunogenic cell death-related risk signature predicts prognosis and characterizes the tumour microenvironment in lower-grade glioma. *Front Immunol.* 2022;13:1011757.
51. Chen Y, Zhao S, Kang Y, Zhang Y, Chang X. Identification of immune infiltration landscape on prognosis and therapy of the ferroptosis-related genes signature in breast cancer. *Biochim Biophys Acta Mol Cell Res.* 2022;1869(11): 119328.
52. Li Y, Du Y, Zhou Y, Chen Q, Luo Z, Ren Y, et al. Iron and copper: critical executioners of ferroptosis, cuproptosis and other forms of cell death. *Cell Commun Signal.* 2023;21(1):327.
53. Xue Q, Yan D, Chen X, Li X, Kang R, Klionsky DJ, et al. Copper-dependent autophagic degradation of GPX4 drives ferroptosis. *Autophagy.* 2023;19(7):1982–96.
54. Cafri G, Gartner JJ, Zaks T, Hopson K, Levin N, Paria BC, et al. mRNA vaccine-induced neoantigen-specific T cell immunity in patients with gastrointestinal cancer. *J Clin Invest.* 2020;130(11):5976–88.
55. Gu YZ, Zhao X, Song XR. Ex vivo pulsed dendritic cell vaccination against cancer. *Acta Pharmacol Sin.* 2020;41(7):959–69.
56. Shahnazari M, Samadi P, Pourjafar M, Jalali A. Therapeutic vaccines for colorectal cancer: the progress and future prospect. *Int Immunopharmacol.* 2020;88: 106944.
57. Chang X, Miao J. Ferroptosis: mechanism and potential applications in cervical cancer. *Front Mol Biosci.* 2023;10:1164398.
58. Monk BJ, Enomoto T, Kast WM, McCormack M, Tan DSP, Wu X, et al. Integration of immunotherapy into treatment of cervical cancer: recent data and ongoing trials. *Cancer Treat Rev.* 2022;106: 102385.
59. Jin W, Liu J, Yang J, Feng Z, Feng Z, Huang N, et al. Identification of a key ceRNA network associated with ferroptosis in gastric cancer. *Sci Rep.* 2022;12(1):20088.

60. Han S, Wang S, Lv X, Li D, Feng Y. Ferroptosis-related genes in cervical cancer as biomarkers for predicting the prognosis of gynecological tumors. *Front Mol Biosci.* 2023;10:1188027.
61. Tang W, Xu F, Zhao M, Zhang S. Ferroptosis regulators, especially SQLE, play an important role in prognosis, progression and immune environment of breast cancer. *BMC Cancer.* 2021;21(1):1160.
62. Ji Y, Liu L, Liu Y, Ma Y, Ji Z, Wu X, et al. Exploring gene biomarkers and targeted drugs for ferroptosis and cuproptosis in osteosarcoma: a bioinformatic approach. *Environ Toxicol.* 2024. <https://doi.org/10.1002/tox.24250>.
63. Jiang L, Kon N, Li T, Wang SJ, Su T, Hibshoosh H, et al. Ferroptosis as a p53-mediated activity during tumour suppression. *Nature.* 2015;520(7545):57–62.
64. Xiong C, Ling H, Hao Q, Zhou X. Cuproptosis: p53-regulated metabolic cell death? *Cell Death Differ.* 2023;30(4):876–84.
65. Zhu W, Feng D, Shi X, Li D, Wei Q, Yang L. A pan-cancer analysis of the oncogenic role of zinc finger protein 419 in human cancer. *Front Oncol.* 2022;12:1042118.
66. Wu J, Minikes AM, Gao M, Bian H, Li Y, Stockwell BR, et al. Intercellular interaction dictates cancer cell ferroptosis via NF2-YAP signalling. *Nature.* 2019;572(7769):402–6.
67. Huang N, Wei Y, Cheng Y, Wang X, Wang Q, Chen D, et al. Iron metabolism protein transferrin receptor 1 involves in cervical cancer progression by affecting gene expression and alternative splicing in HeLa cells. *Genes Genom.* 2022;44(6):637–50.
68. Zhao MY, Liu P, Sun C, Pei LJ, Huang YG. Propofol augments paclitaxel-induced cervical cancer cell ferroptosis in vitro. *Front Pharmacol.* 2022;13:816432.
69. Guo W, Yu H, Zhang L, Chen X, Liu Y, Wang Y, et al. Effect of hyperoside on cervical cancer cells and transcriptome analysis of differentially expressed genes. *Cancer Cell Int.* 2019;19:235.

Publisher's Note

Springer Nature remains neutral with regard to jurisdictional claims in published maps and institutional affiliations.